Viscoelastic properties of the human abdominal adipose tissue

Jose L Calvo-Gallego[a,d,*], Jaime Domínguez[a], Tomás Gómez Cía[b], Gorka Gómez Ciriza[c], Javier Martínez-Reina[a]

[a]*Department of Mechanical Engineering, University of Seville, Camino de los Descubrimientos s/n, Seville 41092, Spain*
[b]*Cirugía Plástica y Grandes Quemados, Hospital Virgen del Rocío, Seville, Spain*
[c]*Grupo de Innovación Tecnológica, Hospital Virgen del Rocío, Seville, Spain*
[d]*Fundación Ayesa, Avd. Marie Curie 2, PCT Cartuja, Seville 41092, Spain*

Abstract

This is a preprint of the paper, written before peer review. The reader is referred to the published version of this paper: https://doi.org/10.1016/j.jmbbm.2018.02.013. Please, cite this work as: J.L. Calvo-Gallego, J. Domínguez, T. Gómez Cía, G. Gómez Ciriza and J. Martínez-Reina. Comparison of different constitutive models to characterize the viscoelastic properties of human abdominal adipose tissue. A pilot study. Journal of the Mechanical Behavior of Biomedical Materials. 2018; 80:293-302.

Knowing the mechanical properties of human adipose tissue is key to simulate surgeries such as liposuction, mammoplasty and many plastic surgeries in which the subcutaneous fat is present. One of the most important surgeries, for its incidence, is the breast reconstruction surgery that follows a mastectomy. In this case, achieving a deformed shape of the breast similar to the healthy breast is crucial. The reconstruction is most commonly made using autologous tissue, taken from the patient's abdomen. The amount of autologous tissue and its mechanical properties have a strong influence on the shape of the reconstructed breast. In this work, the viscoelastic mechanical properties of the human adipose tissue have been studied. Uniaxial compression stress relaxation tests were performed in adipose tissue specimens extracted from the human abdomen. Two different viscoelastic models were used to fit to the experimental tests: a quasi-linear viscoelastic (QLV) model and an internal variables viscoelastic (IVV) model; each one with four different hyperelastic strain energy density functions to characterise the elastic response: a 5-terms polynomial function, a first order Ogden function, an isotropic Gasser-Ogden-Holzapfel function and a combination of a neo-Hookean and an exponential functions. The IVV model with the Ogden function was the best combination to fit the experimental tests. The viscoelastic properties are not important in the simulation of the static deformed shape of the breast, but they are needed in a relaxation test performed under finite strain rate, particularly, to derive from that test the stiffness as time tends to infinity, needed to estimate the static deformed shape of the breast. The stiffness so obtained was compared with previous results given in the literature for adipose tissue of different regions, which exhibited a wide dispersion.

Keywords:

human adipose tissue, abdomen, stress relaxation test, viscoelasticity, mechanical properties

1. Introduction

The adipose tissue is involved in many surgeries. For instance, in plastic surgery, in which fat is always present as subcutaneous adipose tissue or in liposuction, in which the aim is to eliminate it. In other cases, the adipose tissue is removed from one anatomical site to be implanted in a different one. This is the case of breast reconstruction with autologous tissue, such as for example the deep inferior epigastric artery perforator flap surgery (DIEAP). In this surgery, after a mastectomy is performed in the women breast due to cancer, the breast is reconstructed using tissue from the patient's abdomen. The advantage of this technique against prosthetic breast reconstruction is that the risk of rejection is minimized. Although DIEAP surgery is more expensive and needs a longer surgical time than breast tissue expander and prostheses surgeries, recent studies have showed that the former is cost-effective in comparison to the latter [30, 33]. One aim of the reconstruction is mimicking the deformed shape of the healthy breast and that is influenced by the amount of implanted tissue and its mechanical properties. Therefore, the assessment of these properties is key in Finite Element (FE) simulations of the surgery, which may help in pre-operative planning.

Many examples of these FE simulations can be found in the literature: to predict the location of a tumour [2, 40]; to simulate the compression of the breast between two plates, like in a mammography [2, 21, 38, 40, 46]; for image registration, normally performing also a compression [20, 25–27, 35, 43, 44, 49]; to simulate the deformed shape under gravity loading in standing position [16, 39, 41, 42, 55]; to simulate a prosthesis insertion for augmentation mammoplasty [32], etc. Moreover, some FE models can be found addressing the mechanical properties of the fat of other anatomical sites, like the calcaneal fat pad [34, 37]. Probably, the main limitation of these studies is the lack of a solid knowledge of the mechanical properties of the body fat.

The adipose tissue is a loose connective tissue in which adipocytes are the main cellular component. Adipocytes are separated and supported by connective tissue septa. The adipose tissue plays a fundamental role in energy homeostasis, but it also has a structural function, serving as a padding to protect other organs.

Most authors have considered the adipose tissue as isotropic, in computational simulations [2, 16, 20, 25–27, 32, 38–44, 46, 49, 55] as well as fitting experimental tests [7–9, 36, 45, 47, 48, 50, 52]. Recently, Sommer et al. [51] considered it as an anisotropic material with one family of fibers, by identifying a preferential direction in the connective tissue that surrounds the adipocytes. However, those authors gave no reason to consider only one family of fibers. Furthermore, they did not determine the fiber direction through histological studies, but in a phenomenological

*Corresponding author. Tel.: +34-954487311; fax: +34-954460475.
Email address: joselucalvo@us.es (Jose L Calvo-Gallego)

way. Therefore, it is difficult to use this fibred model in a FE simulation. All the previously cited works considered adipose tissue as an incompressible material. Finally, there are some studies in which the viscoelastic behaviour of the adipose tissue has been clearly identified and described [51].

As stated above, there is not much information in the literature about the mechanical properties of the adipose tissue, let alone for the human adipose tissue. The most studied animal tissue has been porcine subdermal fat. Geerligs et al. [18] performed shear tests on this tissue with a special focus on its viscoelastic behaviour. In the linear viscoelastic regime, they analysed the storage and loss modulus and its dependency on temperature and frequency. They also introduced a power law function to describe the frequency dependent behaviour and the stress relaxation behaviour. Comley and Fleck [8, 9] performed shear and uniaxial compression tests in a wide range of strain rates. They fitted a first order Ogden model to the experimental results. These authors also studied the toughness of this tissue [10]. Sims et al. [50] performed indentation tests, fitting a neo-Hookean model with Prony series to model the time dependent behaviour. Few authors have studied human adipose tissue. Bennett and Ker [3] carried out indentation tests on the heel pad from amputated limbs, showing the force-displacement relation but not providing any model to fit the experimental results. Miller-Young et al. [36] performed quasi-static and relaxation compression tests on human cadaveric heel pads. They fitted the results using a Mooney-Rivlin model and an exponential decay to account for the change in the material constants over time. Samani et al. performed indentation tests on human breast fat, modelling it as a linear elastic material [45, 48] and as a hyperelastic material modelled with a 5-terms polynomial strain energy density (SED) function [47]. Chen and Weiland [7] carried out uniaxial tension tests on the orbital fat of pigs and humans. They fitted the results with a linear elastic model. Then et al. [52] performed *in vivo* cyclic indentation and relaxation tests in human gluteal tissue. They used a computational simulation to fit a quasi-linear viscoelastic (QLV) model to the skin and fat (considered as a unique material) and the muscle (only the passive state). Sommer et al. [51] carried out biaxial and shear tests on human abdominal adipose tissue and fitted the results using the Gasser-Ogden-Holzapfel (GOH) hyperelastic model with one family of fibers.

As can be seen in those works, there are not many studies about human adipose tissue. Most of them were carried out on the heel pad and only one in the abdominal fat, which is key for the breast reconstruction. Concerning the viscoelastic properties, although some authors has highlighted the viscous behaviour of the adipose tissue, few works have studied such properties. Therefore, little knowledge exists about the viscoelastic properties of human adipose tissue, despite their importance in breast reconstruction.

The aim of this work is to characterize the viscoelastic behaviour of the human adipose tissue, using two different viscoelastic models and several SED functions for the elastic part of the response, in order to choose the most adequate combination of models (visco and elastic). To the author's knowledge, this is the first work that provides the

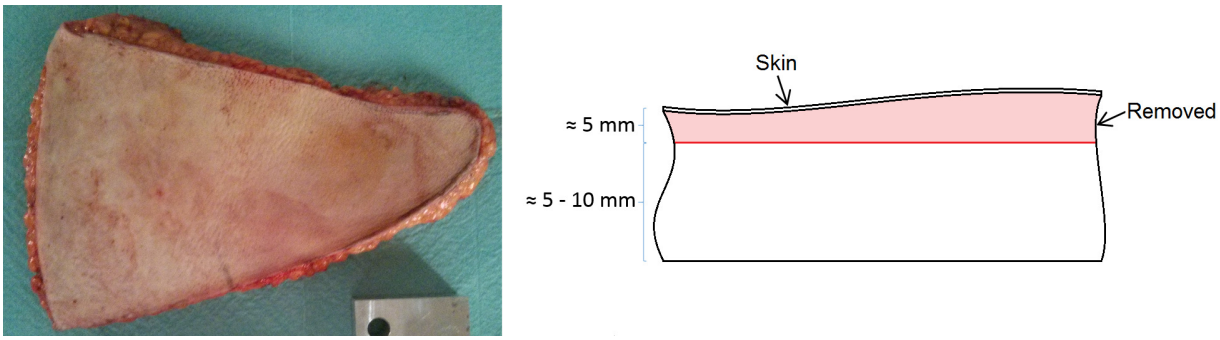

Figure 1: Piece of abdominal adipose tissue from which specimens were extracted. The most superficial layer (in light red) was removed to obtain a sample with parallel faces.

viscoelastic properties of the human abdominal adipose tissue. These properties will aid to improve the FE simulations of process in which this tissue is involved, for example, breast reconstruction with autologous tissue.

2. Materials and methods

2.1. Test protocol

2.1.1. Preparation of specimens

The adipose tissue samples were extracted from the abdomen of a 57 years old female patient subjected to a DIEAP surgery. Specifically, they were extracted from a piece of adipose tissue removed from the abdomen, but not eventually used for the reconstruction (see figure 1).

The pieces were transported from the hospital to the laboratory in a cool-box with dry ice right after the surgery. In less than 30 minutes the pieces were in the laboratory where the skin and the most superficial fat layer were removed by cutting a slice of tissue (or flap) of approximately 5 mm in depth (see figure 1), ensuring that the piece had approximately parallel faces. Depending on the thickness of the extracted abdominal flap, the height of the tested specimens ranged from 5 to 10 mm, which is equal or lower than that used by Miller-Young et al. [36], and was limited to that range to prevent specimens from buckling during the compression tests. The adipose tissue is very soft at room temperature and, consequently, it was difficult to obtain a slice of parallel faces by cutting it at that temperature. Thus, the slice was cut while the tissue was thawing.

The reconstruction surgery is quite long and, consequently, the mechanical test could not be performed the same day of extraction. Thus, the slice was frozen to avoid degradation of the tissue. It was wrapped in saline-soaked gauze (saline solution: 0.9% w/v of NaCl); wrapped in a plastic film and introduced in hermetic vials to prevent dehydration; and finally frozen at $-20°$C until the following day, when the tests were carried out.

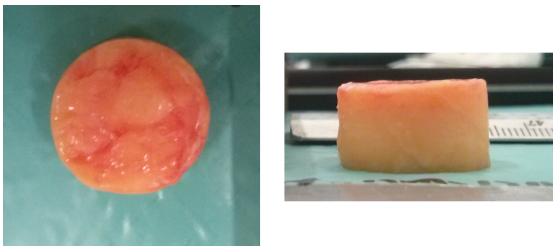

Figure 2: Cylindrical specimen, top and lateral view.

The mechanical tests were performed in cylindrical specimens that were extracted from the slice by slowly pushing a hollow punch of 19 mm in diameter against the slice. This extraction had to be done while the slice was frozen. Otherwise, the final shape of the specimens was irregular and far from cylindrical, because the tissue was largely deformed by the punch. A specimen with the final cylindrical shape can be seen in figure 2. Next, the specimen was submerged in saline solution at room temperature and allowed to thaw. Then, it was digitally photographed to measure its cross-sectional area through computerised image analysis.

2.1.2. Relaxation test

The specimens were subjected to a relaxation test under unconfined uniaxial compression between two platens. A servo-hydraulic testing machine (858 Mini Bionix II, MTS, Eden Prairie, USA) was used to apply the compression. To ensure that the test was performed under physiologic conditions of humidity and temperature, the experimental setup, shown in figure 3, included a methacrylate recipient filled with saline solution, that was kept at 37 ± 1 °C by means of a heater and thermostat. This experimental setup was already used in a previous study in which the same test was performed on temporomandibular articular discs [11].

To perform the tests the following procedure was followed. First, both platens of the testing machine were brought into contact to zero the displacement. Then, the upper platen was moved upward and some vaseline was spread on the surface of both platens to reduce friction and facilitate the sliding of the specimens. Once the specimen was thawed, it was placed at the center of the inferior platen of the testing machine. Unlike in the previous work referred to above [11], the specimen was not glued to the inferior platen to prevent it from slipping off. In this case, gluing was not necessary to keep the specimens between the platens and, besides, this allowed to get a stress state closer to uniaxial [12]. Next, the upper platen was moved downwards, slowly approaching the sample, and visually positioned in contact with the top surface of the sample, as made in [36]. That allowed to measure the thickness of the specimen and to define the starting point of the test.

A preconditioning load was applied to each sample consisting in 20 cycles from 0% to 10% strain at 1 Hz, like in [1]. This was followed by a ramp from 0% to 50% strain, like in [11, 36]. This final strain was maintained for 15 min,

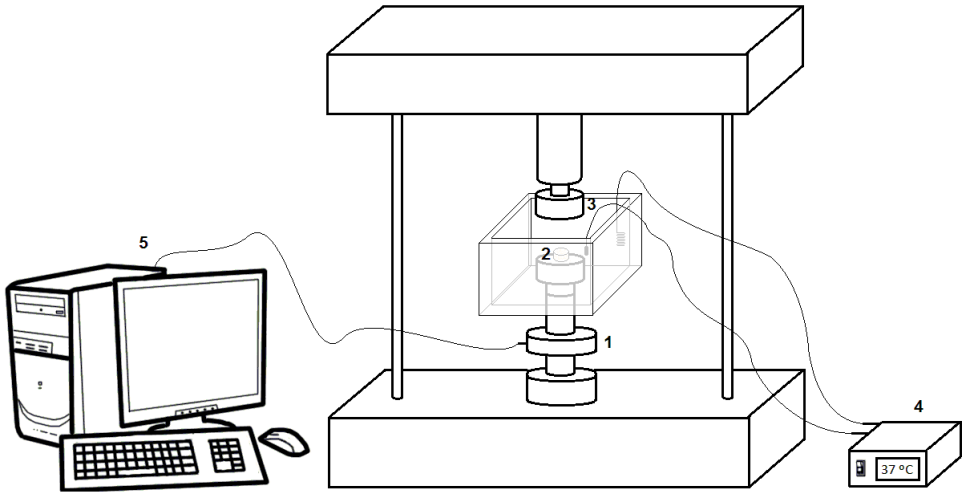

Figure 3: Diagram of the test. Remarked: (1) loading cell, (2) sample, (3) upper platen, (4) temperature controller, (5) acquisition system.

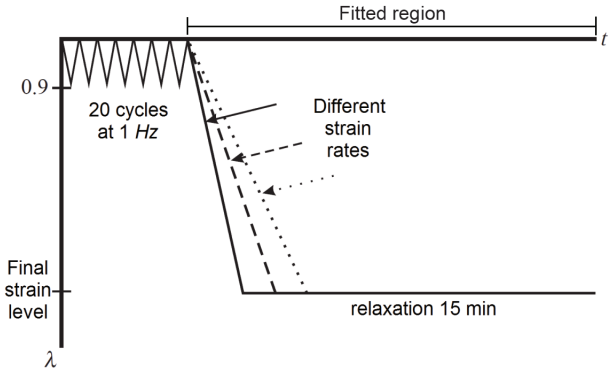

Figure 4: Scheme of the evolution of the stretch with time in the relaxation test.

allowing for stress relaxation (see figure 4). The strain level used here corresponds to the breast compression reported by some authors [21, 44]. Different strain rates were applied for the loading ramp: 50%, 60% and 70%/s, which are in the range used by other authors [36].

The applied force, $F(t)$, and the displacement of the upper platen $u(t)$ were continuously recorded during the test. The lower platen was fixed. From these data, the experimental Cauchy stress, $\overline{\sigma}$, was estimated assuming uniaxial compression, through:

$$\overline{\sigma}(t) = \frac{F(t)\ \lambda(t)}{A_0}, \qquad \lambda(t) = 1 + \frac{u(t)}{L_0} \tag{1}$$

where A_0 is the initial cross-sectional area of the sample and L_0 is the initial length of the specimen. The experimental stress record was fitted using two different viscoelastic models described hereunder.

2.2. Data fitting algorithm: quasi-linear viscoelastic model

The quasi-linear viscoelastic (QLV) model has been widely used to model the behaviour of soft tissues [6, 11, 14, 15, 54]. For a general stretch history, $\lambda = \lambda(t)$, the temporal evolution of stress is given by equation (2). Here, the stretch history is given in figure 4, but it must be noted that the preconditioning cycles were dismissed from the stress record (the finally fitted region is indicated in figure 4).

$$\sigma(t) = \int_0^t \overline{G}(t-\tau)\,\frac{dT^e(\lambda)}{d\lambda}\,\frac{d\lambda(\tau)}{d\tau}\,d\tau \tag{2}$$

The reduced stress relaxation function $\overline{G}(t)$ is given by a five-terms Prony series like in [31]:

$$\overline{G}(t) = g_\infty + \sum_{i=1}^{5} g_i\, e^{-t/\tau_i} \tag{3}$$

normalized such that:

$$\overline{G}(0) = g_\infty + \sum_{i=1}^{5} g_i = 1 \tag{4}$$

The relaxation time constants were taken in decades: $\tau_1 = 0.01\ s$, $\tau_2 = 0.1\ s$, $\tau_3 = 1\ s$, $\tau_4 = 10\ s$ and $\tau_5 = 100\ s$ [29], fixed *a priori* to ensure the uniqueness of the fitted function $\overline{G}(t)$ [53].

The elastic response function, $T^e(\lambda)$, provides the instantaneous stress response to a uniaxial stretch step λ and was formulated here using incompressible hyperelastic models. Four SED functions were tried: a polynomial function with 5 terms[1], Ψ_{pol}, the first order Ogden model, Ψ_{Og}, the GOH model [17], Ψ_{GOH}, in its isotropic version and a combination of a neo-Hookean model and an exponential one, Ψ_{exp} (see table 1).

As explained in [11], the raw stress record, $\overline{\sigma}$, was treated in two steps:

1. At the beginning of the test, the upper platen might not be in full contact with the sample, causing a zero or even a positive initial slope in the stress - stretch curve in some samples, resulting in a spurious toe region. This produced certain numerical problems in the fitting of the experimental stress. Therefore, this spurious toe region was eliminated, with an iterative algorithm designed in [11].
2. The record was filtered using a moving average filter to improve the shape of the curve.

The resulting stress record, named here $\tilde{\sigma}$, was fitted to the analytical stress record, σ, given through equation (2) by using a least squares method that minimizes the following quadratic error:

[1] It includes polynomial functions with less number of terms if any fitted constant is zero.

SED	Elastic response function
$\Psi_{\text{pol}} = C_{10}(I_1-3) + C_{01}(I_2-3) +$	$T^e_{\text{pol}} = 2C_{10}\,(\lambda^2 - \frac{1}{\lambda}) + 2C_{01}\,(\lambda - \frac{1}{\lambda^2}) + 6C_{11}\,(\lambda^3 - \lambda^2 - \lambda +$
$+C_{11}(I_1-3)(I_2-3) +$	$+\frac{1}{\lambda} + \frac{1}{\lambda^2} - \frac{1}{\lambda^3}) + 4C_{20}\,(\lambda^4 - 3\lambda^2 + \lambda + \frac{3}{\lambda} - \frac{2}{\lambda^2}) +$
$+C_{20}(I_1-3)^2 + C_{02}(I_2-3)^2$	$+4C_{02}\,(2\lambda^2 - 3\lambda - \frac{1}{\lambda} + \frac{3}{\lambda^2} - \frac{1}{\lambda^4})$
$\Psi_{\text{Og}} = \frac{\mu}{\alpha}(\lambda_1^\alpha + \lambda_2^\alpha + \lambda_3^\alpha - 3)$	$T^e_{\text{Og}} = \mu\,(\lambda^\alpha - \frac{1}{\lambda^{\frac{\alpha}{2}}})$
$\Psi_{\text{GOH}} = C_{10}(I_1-3) + \frac{k_1}{2k_2}[e^{k_2(I_1-3)^2} - 1]$	$T^e_{\text{GOH}} = 2(C_{10} + k_1(\lambda^2 + \frac{2}{\lambda} - 3)\,e^{k_2(\lambda^2+\frac{2}{\lambda}-3)^2})\,(\lambda^2 - \frac{1}{\lambda})$
$\Psi_{\text{exp}} = C_{10}(I_1-3) + \frac{k_1}{k_2}[e^{k_2(I_1-3)} - 1]$	$T^e_{\text{exp}} = 2(C_{10} + k_1\,e^{k_2(\lambda^2+\frac{2}{\lambda}-3)^2})\,(\lambda^2 - \frac{1}{\lambda})$

Table 1: SED functions and the corresponding elastic response functions.

$$e = \sum_{i=1}^{N} \left(\tilde{\sigma}(t_i) - \sigma(t_i)\right)^2 \tag{5}$$

where N is the total number of points recorded during the relaxation test and t_i is the time elapsed since the beginning of the test at point i. The goodness of the least squares fitting was evaluated by means of the coefficient of variation, CV:

$$CV(\%) = \frac{\sqrt{\frac{\sum_{i=1}^{N}\left(\sigma(t_i) - \tilde{\sigma}(t_i)\right)^2}{N}}}{\mu_{\tilde{\sigma}}} \times 100 \tag{6}$$

where $\mu_{\tilde{\sigma}}$ is the mean value of the temporal record $\tilde{\sigma}(t_i)$.

2.3. Data fitting algorithm: internal variables viscoelastic (IVV) model

With the internal variables viscoelastic (IVV) model, the structure of the algorithm is the same that in the previous section, though with different equations. Many authors have used this IVV approach to model different materials [22], or its extension to fibred models presented in [23]. In this IVV model, the second Piola-Kirchhoff stress tensor takes the form:

$$\mathbf{S} = \mathbf{S}^{\infty}_{\text{vol}} + \mathbf{S}^{\infty}_{\text{iso}} + \sum_{j=1}^{m} \mathbf{Q}_j \tag{7}$$

with $\mathbf{S}^{\infty}_{\text{vol}}$ and $\mathbf{S}^{\infty}_{\text{iso}}$ the fully elastic volumetric and isochoric contributions to the second Piola-Kirchhoff stress tensor respectively, and $\mathbf{Q}_j$ representing the non-equilibrium stresses. The evolution equations for these internal variables are:

$$\dot{\mathbf{Q}}_j + \frac{\mathbf{Q}_j}{\tau_j} = \dot{\mathbf{S}}_{\text{iso}\,j} \tag{8}$$

where τ_j is the relaxation time, which play the same role as τ_i in the QLV model, and $\mathbf{S}_{\text{iso}\,j}$ is the isochoric second Piola-Kirchhoff stress tensor which corresponds to the isochoric strain energy function $\Psi_{\text{iso}\,j}$, responsible for the j relaxation process and defined in the subsequent equations. The solution of the differential equation 8 for $t \in (0, T]$ is:

$$\mathbf{Q}_j = e^{-T/\tau_j}\mathbf{Q}_{j\,0^+} + \int_{t=0^+}^{t=T} e^{-(T-t)/\tau_j}\dot{\mathbf{S}}_{\text{iso}\,j}(t)dt \tag{9}$$

where $\mathbf{Q}_{j\,0^+}$ is the instantaneous stress response appearing at $t = 0^+$. If the following assumption is made [22]:

$$\Psi_{\text{iso}\,j}(\bar{\mathbf{C}}) = \beta_j^{\infty}\Psi_{\text{iso}}^{\infty}(\bar{\mathbf{C}}) \tag{10}$$

where $\Psi_{\text{iso}}^{\infty}$ is the isochoric SED when time tends to infinity, and $\bar{\mathbf{C}} = \bar{\mathbf{F}}^T\bar{\mathbf{F}}$ is the modified right Cauchy-Green tensor. $\bar{\mathbf{F}} = J^{-1/3}\mathbf{F}$ is the modified deformation gradient tensor, with $\mathbf{F}$ the deformation gradient tensor and J the volume ratio.

With the assumption (10), the stress $\mathbf{S}_{\text{iso}\,j}$ can be simplified as:

$$\mathbf{S}_{\text{iso}\,j} = \beta_j^{\infty}\mathbf{S}_{\text{iso}}^{\infty}(\bar{\mathbf{C}}) \tag{11}$$

The β_j^{∞} constants are dimensionless strain energy factors. The Cauchy stress tensor is obtained from equation (7), by using the relation $\boldsymbol{\sigma} = J^{-1}\mathbf{F}\mathbf{S}\mathbf{F}^T$. For the non-equilibrium forces $\mathbf{Q}_j$, 5 terms were selected by analogy with the previously presented QLV model (i.e. $j = 1, ..., 5$). As previously, the relaxation time constants, τ_j, were fixed *a priori* to ensure the uniqueness of the fitted set of constants and taken in the same decades: $\tau_1 = 0.01\ s$, $\tau_2 = 0.1\ s$, $\tau_3 = 1\ s$, $\tau_4 = 10\ s$ and $\tau_5 = 100\ s$.

Also, the same four SED functions used with the QLV model were used with the IVV model. With the stretch temporal evolution, $\lambda = \lambda(t)$, shown in figure 4, $\mathbf{S}_{\text{vol}}^{\infty}$ and $\mathbf{S}_{\text{iso}}^{\infty}$ can be calculated, and therefore $\mathbf{Q}_j$ using equation (9). The preconditioning cycles were not considered in the fitting algorithm either. For the implementation of these equations, the algorithm proposed in [24] has been followed.

The treatment of the experimental stress record (elimination of the spurious toe region and filtering of the record), the least squares fitting method and the evaluation of the fitting goodness through the CV were exactly the same that with the QLV model.

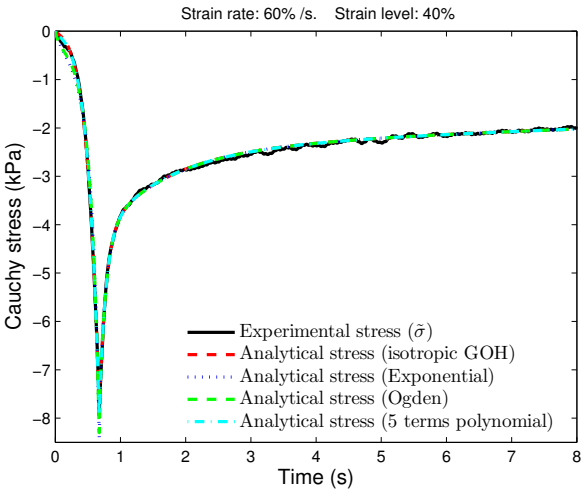

Figure 5: Example of an experimental stress record fitted with the QLV model and different SED functions for the elastic response.

2.4. Performed tests

Following the test protocol and the fitting algorithm explained before, the viscoelastic properties of the human abdominal fat were determined. The number of specimens used for each strain rate was: 47 for $50\%/s$, 45 for $60\%/s$ and 46 for $70\%/s$.

First, the four proposed SED functions were compared to check which one fitted best the experimental curves for each viscoelastic model. The goodness of the fitting was assessed through CV (eq.(6)) and the mean CV was calculated for each SED function using the whole set of specimens $(47+45+46)$. The lowest CV determines the best SED function.

The validity of both, the QLV and the IVV models, was verified for the best SED function selected before. This validity is based on the independence of the fitted material constants with the strain rate. So, the different sets of constants for each strain rate were compared using a statistical test to detect significant differences.

3. Results

3.1. Goodness of fitting of the hyperelastic models with the QLV model

Figure 5 compares a typical experimental stress record, $\tilde{\sigma}$, with the fitting curves for each of the proposed SED functions. In figure 6 a detail of the experimental and fitted stresses obtained during the loading ramp can be seen.

The mean of the CVs, obtained for each specimen is presented in table 2 for each SED function. The CVs were evaluated for the whole test and for the loading ramp separately.

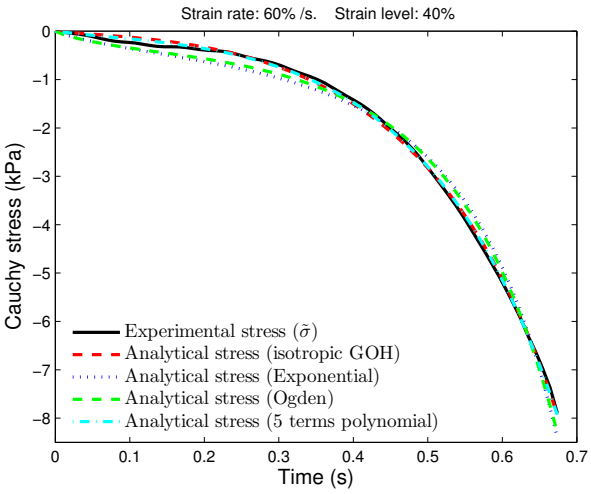

Figure 6: Detail of figure 5 corresponding to the the loading ramp.

Model	Whole test CV (%)	Loading ramp CV (%)
Exponential	4.16	19.88
Ogden	4.05	18.70
GOH	3.06	11.49
Polynomial	2.92	10.67

Table 2: Coefficient of variation of the fitting with the QLV model and the different SED functions.

The polynomial one is a general hyperelastic model, in the sense that it can lead to other models, differently named in the literature, for example, the Mooney-Rivlin model if $C_{11} = C_{20} = C_{02} = 0$. The fitting with the polynomial model was carried out without imposing restrictions to the material constants. For this reason, some of those constants resulted zero for certain specimens. Besides, those zero constants were not systematically the same for all the specimens. Thus, the average model resulted a general five terms polynomial model, but the individual models of each specimen could be different. In other words, the general five terms polynomial model does not seem appropriate to represent the specificity of each specimen and was considered unsuitable, despite producing the lowest CV.

The same occurred to the isotropic GOH model. In many specimens, the fitting led to $k_2 = 0$. In the limit:

$$\lim_{k_2 \to 0} \Psi_{GOH} = C_{10}(I_1 - 3) + \frac{k_1}{2}(I_1 - 3)^2 \tag{12}$$

which is a particular case of the 5 terms polynomial SED function. This is the reason why the GOH and the polynomial models behaved very similarly when fitting the experimental curves. Thus, the isotropic GOH model was also

Strain rate	Quartile	μ (kPa)	α	g_1	g_2	g_3	g_4	g_5	g_∞
50% /s	Q1	3.273	7.584	0.533	0.190	0.039	0.017	0.016	0.013
	Median	4.782	8.424	0.652	0.224	0.049	0.024	0.021	0.018
	Q3	8.436	9.610	0.717	0.316	0.070	0.034	0.032	0.022
60% /s	Q1	2.721	7.490	0.573	0.176	0.038	0.018	0.017	0.013
	Median	6.467	8.361	0.674	0.217	0.048	0.023	0.023	0.017
	Q3	9.588	9.525	0.733	0.298	0.061	0.031	0.030	0.023
70% /s	Q1	3.178	7.456	0.554	0.186	0.041	0.020	0.020	0.014
	Median	5.107	8.437	0.633	0.228	0.047	0.024	0.025	0.018
	Q3	8.786	9.413	0.721	0.280	0.065	0.033	0.032	0.026

Table 3: Median and interquartile range of the QLV constants for the different groups.

considered unsuitable to model the adipose tissue. In view of the foregoing and the average CV, the Ogden model was selected as the best one to represent the behaviour of the adipose tissue from those chosen *a priori*.

3.2. Validity of the QLV model

The validity of the viscoelastic models was proved by checking if the fitted model constants were independent of the strain rate. To do that a multivariate analysis of variance was performed. The categorical independent variable (IV) was the strain rate with three levels: $50\%/s$, $60\%/s$ and $70\%/s$. The dependent continuous variables (DVs) were the seven QLV constants: μ, α, of the Ogden model; and g_1, g_2, g_3, g_4 and g_5 of the Prony series. The constant g_∞ was not included in the statistical analysis because it is a linear combination of the other Prony constants, g_i, due to the normalization condition (4).

To check if the material constants were independent of the strain rate, a non parametric MANOVA (NMANOVA) test was performed, as the stress does not vary linearly with the constant α[1]. Moreover, to apply a parametric MANOVA some assumptions, such as multinormality, need to be checked beforehand. This multinormality was checked for each independent group using the test developed by Cardoso de Oliveira and Ferreira [5]. This test was not significant for the 50% /s group ($p = .098$) and 60% /s group ($p = .160$), but it was for the 70% /s group ($p < .001$) and, thus, multinormality was violated, making it necessary to perform a non-parametric MANOVA (NMANOVA).

In table 3 the median and interquartile range (IQR) for each constant and each strain rate is presented.

The NMANOVA test performed in this work is a multivariate extension of the Kruskal-Wallis test, developed by Katz and McSweeney [28]. Initially, the test was carried out for the 7 aforementioned DVs. No significant differences were found for the three groups compared ($p = .819$). Nonetheless, some authors state that the MANOVA type tests are only indicated if the dependent variables are correlated, but not so strongly correlated ($|R| > .85$) that

[1]For this reason, the median of α represents the sample better than the mean.

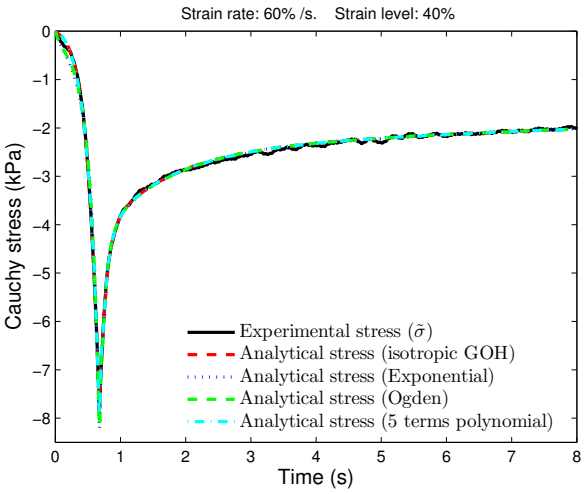

Figure 7: Example of an experimental stress record fitted with the IVV model and different SED functions for the elastic response.

Model	Whole curve CV (%)	Loading ramp CV (%)
Exponential	3.81	17.66
Ogden	3.77	16.99
GOH	3.04	11.36
Polynomial	3.14	12.27

Table 4: Coefficient of variation of the fitting with the IVV model and the different SED functions.

multicollinearity may exist [13, 19]. In this case, constants g_1 and g_2 were strongly correlated and the same occurred to g_3, g_4 and g_5 (Spearman $|R| > .85$ in both cases). So, to be sure of the previous conclusion, the test was repeated after eliminating the correlated variables, that is, for the following 4 DVs: μ, α, g_1 and g_3. The conclusion was the same: there were no statistical differences between the groups ($p = .997$). Therefore, the material constants of the QLV model can be considered independent of the strain rate.

3.3. Goodness of fitting of the hyperelastic models with the IVV model

The same analysis presented before was repeated for the IVV model. Figure 7 compares one of the experimental stress record, $\tilde{\sigma}$, the same shown in figures 5 and 6, with the fitting curves for each of the proposed SED functions. In figure 8 a detail of the experimental and fitted stresses obtained during the loading ramp can be seen.

The mean of the CVs obtained for each specimen is presented in table 4 for each SED function. Again, the CV was evaluated for the whole test and for the loading ramp separately.

As in the QLV model, the fitting with the polynomial and the isotropic GOH SED functions produced some zero constants in certain specimens. For the same reason discussed before, the Ogden model was selected as the best one

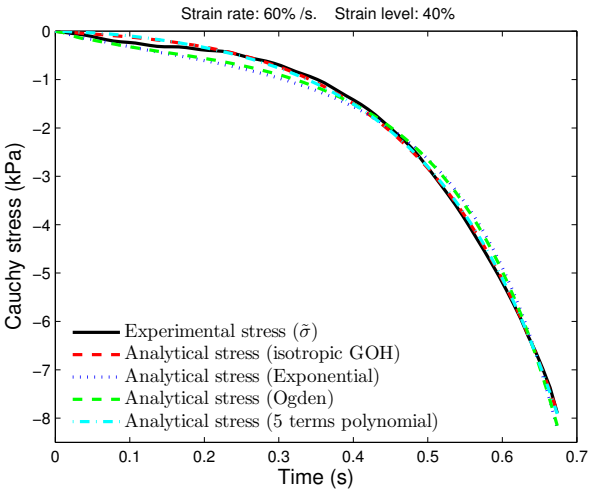

Figure 8: Detail of figure 7 corresponding to the the loading ramp.

to represent the behaviour of the adipose tissue from those chosen *a priori*.

3.4. Validity of the IVV model

As in the section 3.2, the validity of the viscoelastic model was proved by checking if the fitted constants were independent of the strain rate. A NMANOVA test was also carried out, as the stress does not vary linearly with the constant α. Moreover, multinormality was checked for each independent group using the test developed by Cardoso de Oliveira and Ferreira [5]. This test was not significant for the 50% /s group ($p = .534$) and 70% /s group ($p = .205$), but it was for the 60% /s group ($p = .003$) and, thus, multinormality was violated, making necessary to perform a non-parametric MANOVA (NMANOVA). The strain rate was the categorical IV, with three levels ($50\%/s$, $60\%/s$ and $70\%/s$); and 7 DVs: μ, α, β_1^∞, β_2^∞, β_3^∞, β_4^∞ and β_5^∞. The correlation between the DVs was checked, but they were not highly correlated (Spearman $|R| < .85$), so that all of them were considered in the analysis.

In table 5 the median and IQR for each constant and each strain rate is presented. The NMANOVA test developed by Katz and McSweeney [28] showed no significant differences between the three groups compared ($p = .314$). Therefore, the material constants could be considered independent of the strain rate.

4. Discussion

It can be observed in the experimental curves of figures 5 and 6 the presence of a toe region, typical of soft tissues. In normal toe regions the slope of the stress record is initially very small and increases very slightly, for example, in the articular discs of the temporomandibular joint [11]. However, in our case the toe region is not very wide and the

Strain rate	Quartile	μ (kPa)	α	β_1^∞	β_2^∞	β_3^∞	β_4^∞	β_5^∞
50% /s	Q1	0.073	6.920	41.808	9.966	3.193	1.618	1.712
	Median	0.102	8.178	69.189	13.512	3.931	1.993	1.909
	Q3	0.155	9.506	106.125	20.079	4.947	2.551	2.205
60% /s	Q1	0.058	7.117	43.159	9.599	3.262	1.672	1.740
	Median	0.119	8.252	67.712	12.734	3.837	1.981	1.940
	Q3	0.186	9.607	101.241	18.963	4.895	2.383	2.237
70% /s	Q1	0.072	7.110	44.602	8.543	3.162	1.689	1.791
	Median	0.122	8.218	62.563	11.681	3.660	1.987	1.983
	Q3	0.184	9.293	94.787	17.984	4.247	2.539	2.278

Table 5: Median and interquartile range of the IVV constants for the different groups.

loading ramp was quickly noticed by an increase in the compression stress. The relaxation was very quick, with a high percentage (around 70%) of the stress relaxed just a few seconds after the peak and more than 90% of the peak stress relaxed after 15 minutes. Comparing these stress relaxation curves with those obtained by Miller-Young et al. [36], who tested specimens of the human calcaneal fat pad in compression, the peak stress of the present work was of the same order of magnitude and, in both, 75% of the stress was relaxed within the first minute.

It can be seen in figures 5 and 6, that the fitting with the QLV model was quite accurate for the selected specimen. In fact, it was equally accurate for all the specimens and very similar for the four SED functions. It can be noticed that the isotropic GOH and the 5 terms polynomial models fit the experimental curve slightly better than the Ogden and exponential functios, although not too much.

For the QLV model, the best SED function in terms of goodness of fitting, CV, was the polynomial one, closely followed by the GOH function, and a bit farther by the Ogden and exponential functions, in this order (see table 2). In all cases, the CV was quite low for the fitting of the complete stress record. Nonetheless, as discussed before, the polynomial and GOH SED functions were dismissed since they failed to fit all the specimens with the same general equation. For that reason, the Ogden model was eventually selected as the best SED function from those tried in this work.

The high values obtained for the median of g_1 and g_2 (see table 3), corresponding to the relaxation times $\tau_1 = 0.01$ and $\tau_2 = 0.1$, highlight the fast relaxation of the specimens. The sum of both (around 90%) represents the percentage of the peak stress relaxed up to tenths of a second.

Regarding the IVV model, it can be seen in figures 7 and 8 that the fitting was also very accurate for the selected specimen, which was representative of the general trend. Though not shown, it was equally accurate for all the specimens. The four SED functions produced similar results, but the best fitting was achieved with the GOH function,

Quartile	μ (kPa)	α	β_1^∞	β_2^∞	β_3^∞	β_4^∞	β_5^∞
Q1	0.069	7.105	43.995	8.993	3.221	1.681	1.732
Median	0.115	8.215	66.663	12.761	3.836	1.988	1.950
Q3	0.176	9.437	99.0763	18.872	4.790	2.447	2.238

Table 6: Median and interquartile range of the IVV constants for the human abdominal adipose tissue.

closely followed by the polynomial function, and a little bit farther, by the Ogden and exponential ones, in this order, as can be deduced from CV (see 4).

The goodness of the fitting in terms of CV was slightly better with the IVV model than with the QLV model for all the SED functions, except for the polynomial model, in which case it was only slightly worse (compare tables 2 and 4). As in the QLV model, both the polynomial and GOH functions failed to fit all the specimens with the same general equation and, thus, the Ogden model was finally selected as the best SED function for the IVV model, from those tried in this work.

The parameters β_j^∞ are analogous to the Prony constants g_j in the IVV model and are related to the percentage of stress relaxed up to the relaxation time τ_j. It can be seen in table 5 how the median of β_j^∞ decrease with j, e.g. the relaxation occurred very quickly as could be deduced from the QLV model.

The validity of both models, QLV and IVV, was proven by checking that the material constants were independent of the strain rate applied in the test. Given that the IVV model produced a slightly better fitting than QLV model, it can be concluded that the IVV model with an Ogden SED function for the elastic response was the best choice to characterise the abdominal adipose tissue, from the models tried in this work. Therefore, and due to independence of the strain rate, the median and IQR of each constant were calculated for the whole set of specimens and are presented in table 6.

The analyzed specimens were extracted from the same patient and this may seem a limitation of the study, but it was justified for the following reason. In a previous work [4], the viscoelastic properties of the adipose tissue of two patients were compared, finding significant differences between them. That result highlights the specificity of the mechanical properties of the adipose tissue of each individual. The main objective of the present study was validating the use of certain viscoelastic models, which implied comparing the material constants fitted for different strain rates. So, the only variable whose effect was of interest was the strain rate and other sources of scattering, such as inter-individual differences, should be eliminated from the statistical analysis, otherwise they could have hidden the main effect of the strain rate.

5. Conclusion

In the present work, the viscoelastic behaviour of the human adipose tissue has been investigated. Stress relaxation tests at different strain rates were carried out and fitted with two different models, the quasi-linear viscoelastic and the internal variables viscoelastic models. The same four SED functions were used to describe the elastic response in both cases. It was found that all of them provided a good fitting of the experimental result, being the internal variables viscoelastic model with an Ogden SED function the best option. Moreover, the validity of both viscoelastic models was checked by statistically comparing the constants fitted for different strain rates and finding no significant differences between those fitted constants.

Conflict of interest statement

The authors declare that they have no conflict of interest.

Acknowledgements

The authors gratefully acknowledge the research support from the Spanish *'Ministerio de Economía y Competitividad'* through the research project DPI2011-28080, *'Modelado numérico de un proceso de reconstrucción mamaria'*.

References

References

[1] K. D. Allen and K. A. Athanasiou. Viscoelastic characterization of the porcine temporomandibular joint disc under unconfined compression. *Journal of Biomechanics*, 39(5):312–322, 2006.

[2] F. S. Azar, D. N. Metaxas, and M. D. Schnall. A deformable finite element model of the breast for predicting mechanical deformations under external perturbations. *Academic Radiology*, 8:965–975, 2001.

[3] M. B. Bennett and R. F. Ker. The mechanical properties of the human subcalcaneal fat pad in compression. *Journal of Anatomy*, 171:131–138, 1990.

[4] J. L. Calvo-Gallego. *Experimental Characterisation of Breast Tissues and its Application to a Numerical Model of a Healthy Breast*. PhD thesis, Universidad de Sevilla, 2017.

[5] I. R. Cardoso de Oliveira and D. F. Ferreira. Multivariate extension of chi-squared univariate normality test. *Journal of Statistical Computation and Simulation*, 80(5):513–526, 2010.

[6] E. O. Carew, E. A. Talman, D. R. Boughner, and et al. Quasi-linear viscoelastic theory applied to internal shearing of porcine aortic valve leaflets. *Journal of Biomechanical Engineering*, 121:386–392, 1999.

[7] K. Chen and J. D. Weiland. Mechanical properties of orbital fat and its encapsulating connective tissue. *Journal of Biomechanical Engineering*, 133(6), 2011.

[8] K. Comley and N. Fleck. The high strain rate response of adipose tissue. In G. M. L. Gladwell, R. Moreau, H. Zhao, and N. Fleck, editors, *IUTAM Symposium on Mechanical Properties of Cellular Materials*, volume 12, pages 27–33. Springer, Netherlands, 2009.

[9] K. Comley and N. Fleck. The mechanical response of porcine adipose tissue. *ASME Journal of Biomechanical Engineering*, pages 1–30, 2009.

[10] K. Comley and N. Fleck. The toughness of adipose tissue: measurements and physical basis. *Journal of Biomechanics*, 43:1823–1826, 2010.

[11] M. S. Commisso, J. L. Calvo-Gallego, J. Mayo, and et al. Quasi-linear viscoelastic model of the articular disc of the temporomandibular joint. *Experimental Mechanics*, 56(7):1169–1177, 2016.

[12] M. S. Commisso, J. Martínez-Reina, J. Mayo, and et al. Numerical simulation of a relaxation test designed to fit a quasi-linear viscoelastic model for temporomandibular joint discs. *Proceedings of the Institution of Mechanical Engineers, Part H: Journal of Engineering in Medicine*, 227 (2):190–199, 2013.

[13] W. R. Dillon and M. Goldstein. *Multivariate analysis. Methods and applications*. John Wiley & Sons, USA, 1984.

[14] C. S. Drapaca, G. Tenti, K. Rohlf, and et al. A quasi-linear viscoelastic constitutive equation for the brain: application to hydrocephalus. *Journal of Elasticity*, 85:65–83, 2006.

[15] Y. C. Fung. *Biomechanics: Mechanical properties of living tissues*. Spinger-Verlag, New York, 1993.

[16] T. B. Gamage, R. Boyes, V. Rajagopal, and et al. Modelling prone to supine breast deformation under gravity loading using heterogeneous finite element models. In A. Wittek P. M. F. Nielsen and K. Miller, editors, *Computational Biomechanics for Medicine*, pages 29–38. Springer New York, 2012.

[17] T. C. Gasser, R. W. Ogden, and G. A. Holzapfel. Hyperelastic modelling of arterial layers with distributed collagen fiber orientations. *Journal of the Royal Society Interface*, 3:15–35, 2006.

[18] M. Geerligs, G. W. M. Peters, P. A. J. Ackermans, and et al. Linear vicoelastic behaviour of subcutaneous adipose tissue. *Biorheology*, 45:677–688, 2008.

[19] J. F. Hair, R. L. Tatham, R. E. Anderson, and et al. *Multivariate Data Analysis*. Prentice Hall, New Jersey, 1998.

[20] L. Han, J. H. Hipwell, B. Eiben, and et al. A nonlinear biomechanical model based registration method for aligning prone and supine MR breast images. *IEEE Transactions on Medical Imaging*, 33(3):682–694, 2014.

[21] L. Han, J. H. Hipwell, C. Tanner, and et al. Development of patient-specific biomechanical models for predicting large breast deformation. *Physics in Medicine and Biology*, 57:455–472, 2012.

[22] G. A. Holzapfel. *Nonlinear solid mechanics: A continuum approach for engineering*. Wiley, Chichester, England, 2000.

[23] G. A. Holzapfel and T. C. Gasser. A viscoelastic model for fiber-reinforced composites at finite strains: continuum basis, computational aspects and applications. *Computer Methods in Applied Mechanics and Engineering*, 190:4379–4403, 2001.

[24] G. A. Holzapfel, T. C. Gasser, and R. W. Ogden. A new constitutive framework for arterial wall mechanics and a comparative study of materials models. *Journal of Elasticity*, 61:1–48, 2000.

[25] T. Hopp, P. Baltzer, M. Dietzel, and et al. 2D/3D image fusion of X-ray mammograms with breast MRI: visualizing dynamic contrast enhacement in mammograms. *International Journal of Computed Assisted Radiology and Surgery*, 7:339–348, 2012.

[26] T. Hopp, M. Dietzel, P. Baltzer, and et al. Automatic multimodal 2D/3D breast image registration using biomechanical FEM models and intensity-based optimization. *Medical Image Analysis*, 17:209–218, 2013.

[27] T. Hopp, M. Holzapfel, N. Ruiter, and et al. Registration of X-ray mammograms and three-dimensional speed of sound images of the female breast. *SPIE Proceedings*, 7629:1–9, 2010.

[28] B. M. Katz and M. McSweeney. A multivariate Kruskal-Wallis test with post-hoc procedures. *Multivariate Behavioral Research*, 15:281–297, 1980.

[29] J. H. Koolstra, E. Tanaka, and T. M. G. J. van Eijden. Viscoelastic material model for the temporomandibular joint disc derived from dynamic shear test or strain relaxation tests. *Journal of Biomechanics*, 40:2330–2334, 2007.

[30] A. Lagares-Borrego, P. Gacto-Sanchez, P. Infante-Cossio, and et al. A comparison of long-term cost and clinical outcomes between the two-stage sequence expander/prosthesis and autologous deep inferior epigastric flap methods for breast reconstruction in a public hospital. *Journal of Plastic, Reconstructive and Aesthetic Surgery*, 69:196–205, 2016.

[31] M. J. Lamela, Y. Prado, P. Fernandez, and et al. Non-linear viscoelastic model for behavior characterization of temporomandibular joint discs. *Experimental Mechanics*, 51:1453–1440, 2011.

[32] A. Lapuebla-Ferri, A. Pérez del Palomar, J. Herrero, and et al. A patient-specific FE-based methodology to simulate prosthesis insertion during an augmentation mammoplasty. *Medical Engineering & Physics*, 33:1094–1102, 2011.

[33] E. Matros, C. R. Albornoz, S. N. Razdan, and et al. Cost-effectiveness analysis of implants versus autologous perforator flaps using the breast-q. *Plastic and Reconstructive Surgery*, 135:937–946, 2015.

[34] S. Matteoli, C. G. Fontanella, E. L. Carniel, and et al. Investigation on the viscoelastic behaviour of a human healthy heel pad: In vivo compression tests and numerical analysis. *Proceedings of the Institution of Mechanical Engineers, Part H: Journal of Engineering in Medicine*, 227 (3):216–223, 2013.

[35] T. Mertzanidou, J. Hipwell, S. Johnsen, and et al. MRI to X-ray mammography instensity-based registration with simultaneous optimisation of pose and biomechanical transformation parameters. *Medical Image Analysis*, 18:674–683, 2014.

[36] J. E. Miller-Young, N. A. Duncan, and G. Baroud. Material properties of the human calcaneal fat pad in compression: experiment and theory. *Journal of Biomechanics*, 35:1523–1531, 2002.

[37] A. N. Natali, C. G. Fontanella, and E. L. Carniel. A numerical model for investigating the mechanics of calcaneal fat pad region. *Journal of the mechanical behaviour of biomedical materials*, 5 (1):216–223, 2012.

[38] P. Pathmanathan, D. Gavaghan, J. Whiteley, and et al. Predicting tumour location by simulating large deformations of the breast using a 3-D finite element model and nonlinear elasticity. *Medical Image Computing and Computer-Assisted Intervention*, 2:217–224, 2004.

[39] A. Pérez del Palomar, B. Calvo, J. Herrero, and et al. A finite element model to accurately predict real deformations of the breast. *Physics in Medicine and Biology*, 30:1089–1097, 2008.

[40] S. Pianigiani, L. Ruggiero, and B. Innocenti. An anthropometric-based subject-specific finite element model for the human breast for predicting large deformations. *Frontiers in Bioengineering and Biotechnology*, 3(201):1–9, 2015.

[41] V. Rajagopal, A. Lee, J. H. Chung, and et al. Towards tracking breast cancer across medical images using subject-specific biomechanical models. *Medical Image Computing and Computer Assisted Intervention*, Part I, LNCS 4791:651–658, 2007.

[42] V. Rajagopal, A. Lee, J. H. Chung, and et al. Creating individual-specific biomechanical models of the breast for medical image analysis. *Academic Radiology*, 15:1425–1436, 2008.

[43] N. Ruiter, T. Muller, R. Stotzka, and et al. Automatic image matching for breast cancer diagnostics by a 3-D deformation of the mamma. *Biomedizinische Technik*, 47:644–647, 2002.

[44] N. Ruiter, R. Stotzka, T. Muller, and et al. Model-based registration of X-ray mammograms and MR images of the female breast. *IEEE transactions on nuclear science*, 53:204–211, 2006.

[45] A. Samani, J. Bishop, C. Luginbuhl, and et al. Measuring the elastic modulus of ex vivo small tissue samples. *Physics in Medicine and Biology*, 48:2183–2198, 2003.

[46] A. Samani, J. Bishop, M. J. Yaffe, and et al. Biomechanical 3-D finite element modelling of the human breast using MRI data. *IEEE Transactions on Medical Imaging*, 20:271–279, 2001.

[47] A. Samani and D. Plewes. A method to measure the hyperelastic parameters of ex vivo breast tissue samples. *Physics in Medicine and*

Biology, 49:4395–4405, 2004.

[48] A. Samani, J. Zubovits, and D. Plewes. Elastic moduli of normal and pathological human breast tissues: an inversion-technique-based investigation of 169 samples. *Physics in Medicine and Biology*, 52:1565–1576, 2007.

[49] J. A. Schnabel, C. Tanner, A. D. Castellano-Smith, and et al. Validation of nonrigid image registration using finite-element methods: application to breast MR images. *IEEE Transactions on Medical Imaging*, 22:238–247, 2003.

[50] A. M. Sims, T. Stait-Gardner, L. Fong, and et al. Elastic and viscoelastic properties of porcine subdermal fat using MRI and inverse FEA. *Biomechanics and Modeling in Mechanobiology*, 9:703–711, 2010.

[51] G. Sommer, M. Eder, L. Kovacs, and et al. Multiaxial mechanical properties and constitutive modeling of human adipose tissue: a basis for preoperative simulations in plastic and reconstructive surgery. *Acta Biomaterialia*, 9 (11):9036–9048, 2013.

[52] C. Then, T. J. Vogl, and G. Silber. Method for characterizing viscoelasticity of human gluteal tissue. *Journal of Biomechanics*, 45:1252–1258, 2012.

[53] K. L. Troyer, D. J. Estep, and C. M. Puttlitz. Viscoelastic effects during loading play an integral role in soft tissue mechanics. *Acta Biomaterialia*, 8:234–243, 2012.

[54] S. L-Y. Woo, B.R. Simon, S. C. Kuej, and et al. Quasi-linear viscoelastic properties of normal cartilage. *Journal of Biomechanical Engineering*, 102:85–90, 1980.

[55] M. Zain-Ul-Abdein, F. Morestin, L. Bouten, and et al. Numerical simulation of breast deformation under static conditions. *Cumputer Methods in Biomechanics and Biomedical Enginnering*, 16(S1):50–51, 2013.